


Article

Radium and Lead Radioisotopes Composition of Sediment and Its Biogeochemical Implication in Polymetallic Nodule Area of Clario-Clipperton Zone

Feng Lin ¹ , Cai Lin ¹, Wen Yu ^{2,*}, Xiuwu Sun ¹ and Hui Lin ¹¹ Third Institute of Oceanography, Ministry of Natural Resources, Xiamen 361005, China² School of National Safety and Emergency Management, Beijing Normal University, Zhuhai 519087, China

* Correspondence: yuw@bnu.edu.cn

Abstract: Radioactivity levels of ²¹⁰Pb and ²²⁶Ra were detected in a sediment core obtained using a multi-corer from the polymetallic nodule area inside the Clarion-Clipperton Zone (CCZ), a contract area of the China Ocean Mineral Resources Association (COMR) in the eastern Pacific Ocean. The profile of excess ²¹⁰Pb (²¹⁰Pb_{ex}) shows that the specific activity of ²¹⁰Pb_{ex} has three parts with different distributions at depths of 0–16 cm (I), 17–36 cm (II), and 37–48 cm (III). When the I section of nonlocal mixing was excluded, using a steady-state diffusion mode, the bioturbation coefficients of the core were estimated to be 24.2 cm²/a at 17–36 cm deep and 5.9 cm²/a at 37–48 cm deep, which were greater compared to previously published results. This is most likely owing to bioturbations caused by various organism species in the two sections.

Keywords: radioactivity; ²¹⁰Pb; ²²⁶Ra; bioturbation; sediment core

Citation: Lin, F.; Lin, C.; Yu, W.; Sun, X.; Lin, H. Radium and Lead Radioisotopes Composition of Sediment and Its Biogeochemical Implication in Polymetallic Nodule Area of Clario-Clipperton Zone. *Molecules* **2022**, *27*, 5061. <https://doi.org/10.3390/molecules27165061>

Academic Editors: Jixin Qiao and Galina Lujanienė

Received: 6 July 2022

Accepted: 1 August 2022

Published: 9 August 2022

Publisher's Note: MDPI stays neutral with regard to jurisdictional claims in published maps and institutional affiliations.



Copyright: © 2022 by the authors. Licensee MDPI, Basel, Switzerland. This article is an open access article distributed under the terms and conditions of the Creative Commons Attribution (CC BY) license (<https://creativecommons.org/licenses/by/4.0/>).

1. Introduction

There are approximately 54×10^6 km² of polymetallic nodules in the global oceans, of which the largest area is in the Pacific Ocean, with approximately 23×10^6 km², especially in the Clarion-Clipperton Zone (CCZ) of the eastern Pacific Ocean, which is the most abundant and potentially most economically valuable [1]. The estimated reserves of polymetallic nodules in the CCZ are approximately 21×10^9 t, including approximately 6×10^9 t of Mn, which is larger than all known terrestrial Mn reserves. Meanwhile, the Ni content (270 Mt) and Co content (44 Mt) of polymetallic nodules in the CCZ are three and five times higher than the terrestrial reserves, respectively [2]. With the expansion of the global economy, all nations face a significant resource dilemma, and deep-sea mineral resources dispersed in international public seas are gaining attention from governments and organizations throughout the world.

Traditionally, the primary diagenetic processes of deep-sea polymetallic nodules have been diagenesis and hydrogenesis, but the relevance of biomineral production of deep-sea polymetallic nodules has garnered widespread attention in recent years [3–5]). Furthermore, benthic fauna plays a significant role in the production of both polymetallic nodules and Corich crusts. It is acknowledged that mining and future exploitation would erode the hard substrate and bottom deposition, and may generate sediment plumes, potentially impacting benthic faunal ecosystems across broad regions. Although seabed habitats are particularly vulnerable, data on density, richness, and community structure are missing in many sections of the CCZ [6].

²¹⁰Pb is a naturally occurring radioisotope in the uranium decay series that has been regularly used to assess sedimentation rates and biological mixing records during the last 100 years. The gaseous decay product of its parent ²²⁶Ra, ²²²Rn, escapes from land and decays through a sequence of short-lived daughter bodies to produce ²¹⁰Pb. ²¹⁰Pb remains in the atmosphere for a brief period of time (about 10 days) before migrating out of the

sky via rain, snow, dust, etc. [7,8], and settling on the ocean surface before settling into the sediment, resulting in ^{210}Pb having higher specific activity than its parent ^{226}Ra [9]. Sinking particles convey ^{210}Pb to the bottom, which is produced by the disintegration of ^{226}Ra and ^{222}Rn in the atmosphere and water column. The ^{210}Pb incorporated into the sediment as a result of this process is known as “excess ^{210}Pb ”. The $^{210}\text{Pb}_{\text{ex}}$ signal decays with time, eventually approaching zero after around 100 years. If sediment accumulation alone affects $^{210}\text{Pb}_{\text{ex}}$ distribution, the extra ^{210}Pb signal will be unnoticeable after 100 years, the excess ^{210}Pb relevant to ^{226}Ra indicates a distinct mixing process in the sediments, which was caused by benthic activity [10].

The purpose of this study was to estimate the bioturbation coefficients at the Poly-metallic Nodule Area of CCZ based on high-resolution radionuclide activity distributions in the sediment core.

2. Materials and Methods

2.1. Sampling

On the Monitoring and Protection of Ecology and Environment Cruise in the northeast Pacific in 2017, a sediment core KW1-S05-MC13 was collected on the R/V XIANGYANGHONG03 (Third Institute of Oceanography, MNR, Xiamen, China) (Figure 1, Table 1). Which was discovered at a bottom depth of 5167 m at the sampling site (10.0833° N, −154.3334° E) in the China Ocean Mineral Resources Association’s (COMR) northern polymetallic nodule exploration contract region.

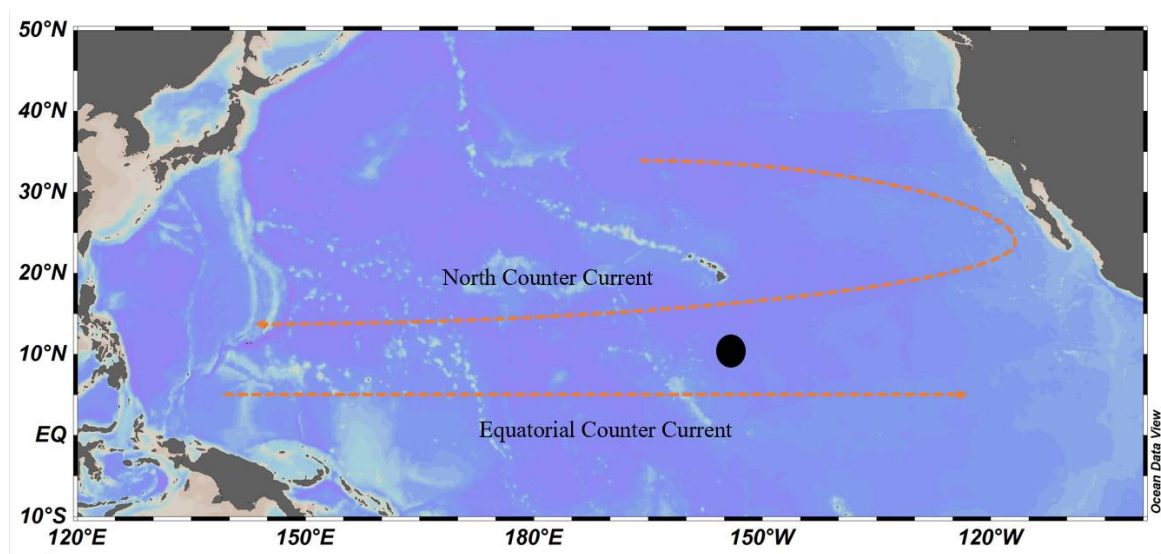


Figure 1. Sampling locations.

Table 1. Coordinates of sampling stations and bioturbation coefficients.

Station	Latitude (°N)	Longitude (°E)	Bottom Depth (m)	D_b (cm^2/a)
KW1-S05-MC13	10.0833	−154.3334	5167	24.2 (II)
				5.9 (III)

The sediment sample was taken using a multi-core sampler with an inner diameter of 9.5 cm, which may gather many undisturbed sediment samples from the seafloor with a deploy, including the sediment-water interface and benthic life. Within 24 h of being collected, the sediment cores were extruded and sectioned at 1 cm intervals. Each subsample was packed individually in a clean polyethylene bag and kept frozen at $-18\text{ }^\circ\text{C}$. The samples were sent to a land-based laboratory for examination.

2.2. ^{210}Pb and ^{226}Ra Analysis

The freeze-dried materials were crushed, pulverized, sieved, and homogenized before being powdered. Due to the detector shield's restricted size, about 2–3 g of the samples was moved to cylindrical plastic containers for gamma spectrometric counting. The cylindrical plastic canisters were sealed for roughly 20 days prior to gamma counting to allow radon and its short-lived progeny to attain secular radioactive equilibrium.

One lead-shielded high-purity germanium (HPGe) detector (Model 9030, Ortec Inc., Atlanta, GA, USA), with an efficiency of 20% and a full width at half maxima (at 1332 keV) less than 2.1, was used for the gamma spectrometry. The characteristic gamma ray used in ^{210}Pb counting is 46.5 keV. The specific radioactivity of ^{210}Pb was calculated according to Formula (1). A self-absorption correction for low-energy ^{210}Pb γ rays was performed following the method described by Cutshall et al. (1983) [11]:

$$A = \sum_{i=1}^n \left(\frac{N_i}{t} - \frac{N_{bi}}{t_b} \right) \times \frac{1}{\varepsilon_i Y_i m} \quad (1)$$

where A is the radioactivity of ^{210}Pb (Bq/kg); N_i and N_{bi} are respectively the counts of the peaks at 46.5 keV of the sample and the blank; t and t_b are the counting times for the sample and blank, respectively; ε_i is the detecting efficiency of ^{210}Pb calibrated with the marine sediment reference material produced by the International Atomic Energy Agency (IAEA-385); m is the mass of the sample (kg); and Y is branch ratio (4.25%).

The radioactivity of ^{226}Ra was derived from the radioactivity levels of its daughter isotopes ^{214}Pb and ^{214}Bi , assuming that they reached equilibrium in the 3-week storage prior to counting. The energy transitions are 295.2 keV (18.4%) of ^{214}Pb and 609.3 keV (45.5%) of ^{214}Bi . The HPGe spectrometer was calibrated for the ^{226}Ra quantitative analysis with the sediment reference material (GBW08304a, produced by the National Center of Reference Material, Beijing, China) containing a known amount of ^{226}Ra .

The acquisition time for the spectrum and the blank were 72 h and 120 h, respectively. All the reported activity values were decay corrected to the date of sample collection.

The excess ^{210}Pb ($^{210}\text{Pb}_{\text{ex}}$), which is the fraction of ^{210}Pb activity exceeding the activity of the parent isotope ^{226}Ra , was determined by subtracting the activity of ^{226}Ra from the activity of ^{210}Pb .

2.3. Quality Controls

10% to 15% of the samples were selected for parallel determination. All the standard deviation of the parallel results was within the permissible range (15%), and then the average of the results was taken as the final result for the specific sample.

Besides, the laboratory has participated in the annual environmental radionuclides analysis proficiency tests organized by the International Atomic Energy Agency (IAEA) and achieved good results, demonstrating that the research team has good quality control in radionuclide measurements.

3. Results

The Distribution of ^{226}Ra and ^{210}Pb

The profiles of ^{226}Ra and ^{210}Pb specific radioactivity are given in Figure 2. The specific radioactivity of ^{226}Ra varied from 298 Bq/kg at the surface to 122 Bq/kg at the bottom, with an average of 214 ± 47 Bq/kg. (The value after the “ \pm ” sign is the uncertainty of the measured result, which depends on the net counting rate obtained in the measuring process and is a characteristic of radioactivity measurement result). The profiles of ^{226}Ra -specific radioactivity in the core decreased gradually with the depth.

The specific radioactivity of ^{210}Pb varied from 525 Bq/kg to 1488 Bq/kg, with an average of 1074 ± 263 Bq/kg. It increased with increasing depth and then descended in an exponential manner with the depth after reaching a maximum at a depth of 18 cm.

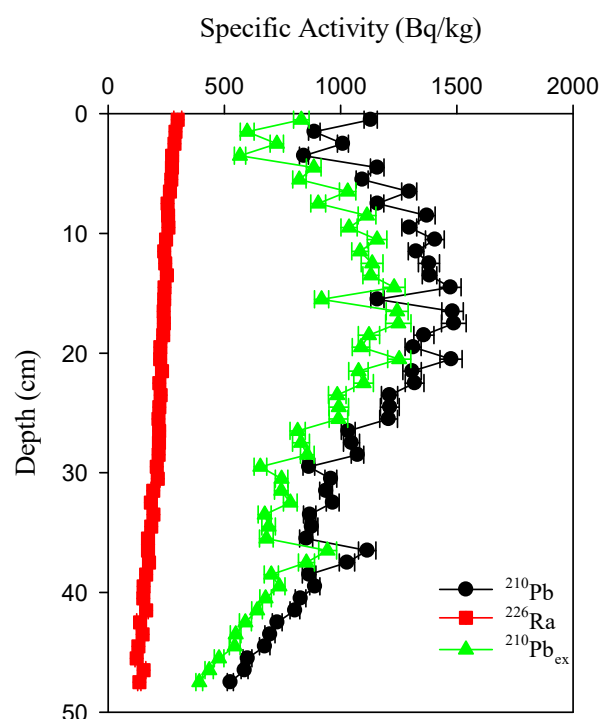


Figure 2. Profiles of ^{210}Pb , ^{226}Ra , and $^{210}\text{Pb}_{\text{ex}}$ specific activity in the sediment core.

4. Discussion

4.1. The Radioactive Disequilibrium between ^{226}Ra and ^{210}Pb

^{210}Pb created in the atmosphere and water column by the decay of ^{226}Ra and ^{222}Rn , was transported on particles to the seafloor by sinking. The ^{210}Pb integrated into the sediment as a result of this process is referred to as “excess ^{210}Pb ”, since it exists in excess of the ^{210}Pb created in situ by the decay of ^{226}Ra and ^{222}Rn within the sediment column (“supported ^{210}Pb ”).

The activity of ^{210}Pb supported by ^{226}Ra is substantially regulated by the activity of ^{230}Th , ^{226}Ra 's parent. Scavenging from the water column and ingrowth from ^{234}U , which is initially in excess due to the high U content of these aragonite-rich sediments, influence ^{230}Th activities in turn.

The main source of ^{210}Pb in deep-sea sediments is the decay of the parent ^{226}Ra . If there are no other processes, the activity distributions of ^{210}Pb and ^{226}Ra should be similar. However, the showed results indicate that the activity of ^{210}Pb did not change with ^{226}Ra . The difference between the two radionuclides indicates that ^{210}Pb is not entirely from the production of ^{226}Ra in the sediment. At the same time, there is a significant excess of ^{210}Pb in the whole column.

The specific radioactivity of $^{210}\text{Pb}_{\text{ex}}$ ranged from 391 Bq/kg to 1252 Bq/kg, with an average of 860 ± 234 Bq/kg. It gradually increases with depth, and reaches a maximum of 20 cm. Then it gradually decreases with depth. But there is an uptick at 36–40 cm.

The significant excess of ^{210}Pb further confirms other sources of ^{210}Pb in the surface sediments. Combined with the strong particle activity of ^{210}Pb , the excess ^{210}Pb should come from ^{210}Pb removed by particulate matter in the bottom water, which would result in a deficit of ^{210}Pb relative to ^{226}Ra in the bottom water. Elevated particulate ^{210}Pb in the Pacific Ocean bottom water supports a stronger particle-scavenging ^{210}Pb process in the bottom water [12,13].

Although the ^{210}Pb removed from the bottom water settled on the sediment surface, a significant excess of ^{210}Pb was still observed in the entire column below the surface to a depth of 48 cm. The sedimentation rate in the vicinity of the study sea area was less than 1 cm/ka. If there is no mixing process, with a half-life of only 22.3 a for ^{210}Pb , it should

reach equilibrium with ^{226}Ra within 1 mm of the surface layer. The actual observations were the opposite, revealing a distinct mixing process in the sediments, which was caused by benthic activity.

Smith and Schafer (1984) used a “conveyor belt” hybrid model to explain the existing ^{210}Pb subsurface sediment maximum value distribution in the North-East Atlantic 4000–5000 m depth [14]; specifically, the benthos feeding is rich in organic matter and radioactive nuclide surface sediment after its discharge to the surface sediment, and the recent single suddenly mixed event model results were consistent with the measured radionuclide section. Smith et al. (1997) discovered $^{210}\text{Pb}_{\text{ex}}$ in deep ocean sediments of the equatorial Pacific Ocean, which displayed a “shoulder phenomenon” at a depth of 23 cm, which researchers suspected was caused by the burrowing operations of huge sea urchins [13]. The equatorial Pacific Ocean’s bottom sediments are densely packed with sea urchins. Sea urchins frequently excavate trenches a few decimeters wide, and they disrupt the surface sediments in these locations every 5 to 7 years [15].

The second largest value of $^{210}\text{Pb}_{\text{ex}}$ in sediments from various Peruvian Sea basin sites emerged at depths of 5–20 cm (the first maximum value was at the surface), which was thought to be generated by surface eating and subsurface excretion of animals such as Echinacea [16]. The Yi insects are responsible for the tropical Pacific Ocean sediments in northeast $^{210}\text{Pb}_{\text{ex}}$ at 22 to 28 cm and 6–10 cm in the subsurface peak, and they rotated the trail of the in situ hybrid [17].

4.2. Bioturbation Coefficient

The quantification of bioturbation is required for the numerical modeling of sediment diagenesis. Using a steady-state diffusion mode, the bioturbation coefficient (D_B) was calculated from the $^{210}\text{Pb}_{\text{ex}}$ activity profile in the sediment. Because of the simple and fast sample measurement, the simultaneous measuring of ^{226}Ra and ^{210}Pb in the sample is capable. Thus the steady-state diffusion mode has been widely applied in studies of sediment bioturbation. In this model, bioturbation and sedimentation are considered to be similar to diffusion and advection. The biological mixing process of tracer material in sediments must fulfill two characteristics when a biological diffusion model is used: (1) The frequency of biological mixing must be significantly larger than the tracer’s disappearance rate, and (2) the particle exchange size must be less than the size of the tracer profile and the thickness of the mixing layer.

Since the half-life of ^{210}Pb is 22.3 a, ^{210}Pb will reach a radioactivity equilibrium with ^{226}Ra in five half-lives (~100 years). Therefore, the $^{210}\text{Pb}_{\text{ex}}$ signal will appear in the sediment that accumulated in the recent period of approximately 100 years. Considering that the sedimentation rates in the study area are estimated to be lower than 1 mm per thousand years, $^{210}\text{Pb}_{\text{ex}}$ should be detectable only within the top 1 mm of the sediment core, if there is no bioturbation or other disturbance. However, in the core samples collected in this study, $^{210}\text{Pb}_{\text{ex}}$ signal was found down to a depth of dozens of centimeters, which was interpreted to be a result of bioturbation. To represent the process of bioturbation, Guinasso and Schink (1975) and Nozaki (1977) devised and modified a steady-state diffusion model [18,19]:

$$\frac{\partial}{\partial t}(\rho A) = \frac{\partial}{\partial z} \left(\rho D_B \frac{\partial A}{\partial z} \right) - \frac{\partial}{\partial z}(\rho S A) - \lambda \rho A \quad (2)$$

where z is the depth of the sediment sample (cm), A is the $^{210}\text{Pb}_{\text{ex}}$ radioactivity (Bq/kg) at the depth of z , ρ is the density (g/cm^3), D_B is the bioturbation coefficient (cm^2/a), S is the sedimentation rate (cm/a), λ is the decay constant of ^{210}Pb (0.031 a^{-1}) and t is the time (a).

Assuming that in the mixing layer, D_B , S and ρ are in a steady state, then $\frac{\partial}{\partial t}(\rho A) = 0$. With the boundary conditions: $A = A_0$ at $z = 0$; and (2) $A \rightarrow 0$ at $z \rightarrow \infty$:

$$A = A_0 \exp \left[\frac{S - \sqrt{S^2 + 4\lambda D_B}}{2D_B} z \right] \quad (3)$$

Since S for oceanic sediments is on the order of mm/ka and the valid time scale of applying ^{210}Pb in tracing bioturbation is approximately 100 a, the sediment deposition process can be ignored, so Equation (3) is simplified as:

$$A = A_0 \exp \left[-z \sqrt{\lambda / D_B} \right] \quad (4)$$

Therefore, the exponential fit of the measured profile of $^{210}\text{Pb}_{\text{ex}}$ quantifies the process of bioturbation.

The depth resolution of radiotracers in this study is very high compared to other research [20–22]. The profile of $^{210}\text{Pb}_{\text{ex}}$ shows that the specific activity of $^{210}\text{Pb}_{\text{ex}}$ has three different distributions at depths of 0–16 cm (I), 17–36 cm (II), and 37–48 cm (III), indicating that the bioturbation coefficient has changed (Figure 3). This suggested that the particle mixing process should be complicated. The complicated vertical profiles were also observed in the Pacific [22,23]. The maximum value in the subsurface layer indicates heterogeneous mixing of particles by benthic organisms [14,24,25]. The $^{210}\text{Pb}_{\text{ex}}$ data affected by nonlocal mixing are excluded when estimating D_B .

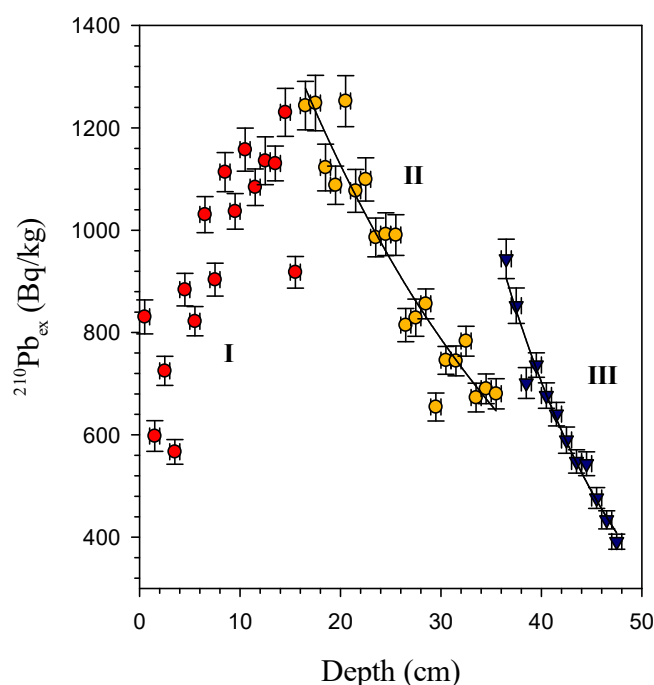


Figure 3. Radioactivity of $^{210}\text{Pb}_{\text{ex}}$ against depth in core samples.

The calculated D_B are $24.2 \text{ cm}^2/\text{a}$ and $5.9 \text{ cm}^2/\text{a}$ in sections II and III, respectively. The D_B values of our research are significantly higher than Yang and Zhou (2004) ($0.26\text{--}2.75 \text{ cm}^2/\text{a}$) [15] and Hyeong et al. (2018) ($1.1\text{--}9.0 \text{ cm}^2/\text{a}$) [20]. On the other hand, it is clear that the D_B of section II is higher than that of section III. The D_B of section III is the same as Hyeong et al. (2018) [20]. This is most likely owing to bioturbations caused by various organism species in the two sections. This will necessitate further investigation in the future.

In the meantime, it should be reminded that it is not reasonable to portray the entire area with the bioturbation coefficients estimated with a single sediment core sample. Although obtaining sediment core from the deep ocean is very cost-consuming, further investigation is needed in the future to better understand the characteristics of this important region.

5. Conclusions

The radioactivity profiles of ^{210}Pb and ^{226}Ra in sediment core from CCZ were measured. A significant $^{210}\text{Pb}_{\text{ex}}$ signal was found throughout the core and has three parts with

different distributions at depths of 0–16 cm (I), 17–36 cm (II), and 37–48 cm (III). Based on the radioactivity profiles of $^{210}\text{Pb}_{\text{ex}}$ in sediment cores from CCZ and the one-dimensional steady-state diffusion model, bioturbation coefficients at one station of different sections were estimated to be $24.2 \text{ cm}^2/\text{a}$ at 17–36 cm deep and $5.9 \text{ cm}^2/\text{a}$ at 37–48 cm deep, which are larger than the reported values, indicating that this region is biologically abundant and has evident bioturbation processes. This is most likely owing to bioturbations caused by various organism species in the two sections. This will necessitate further investigation in the future.

Author Contributions: Conceptualization, F.L. and W.Y.; methodology, F.L. and C.L.; formal analysis, C.L.; investigation, X.S.; resources, H.L.; data curation, F.L.; writing—original draft preparation, F.L.; writing—review and editing, W.Y.; visualization, F.L.; supervision, H.L.; project administration, H.L.; funding acquisition, W.Y. and H.L. All authors have read and agreed to the published version of the manuscript.

Funding: This work was supported by National Natural Science Funding for Young Scholars of China (No. 12105378), BNU Research Start-up Funding for Talent (No. 310432101), the Independent Scientific Research Projects of China Institute for Radiation Protection, the Scientific Research Foundation of Third Institute of Oceanography, MNR (2020012), the Eastern Pacific Eco-environment Monitoring and Protection Project (No. DY-135-E2-5-02), the Guiding Project of the Science and Technology Plan of Fujian Province (No. 2020Y0081), and the COMRA 45 Cruise (DYHC-135-45).

Institutional Review Board Statement: Not applicable.

Informed Consent Statement: Not applicable.

Data Availability Statement: The data presented in this study are available on request from the corresponding author.

Conflicts of Interest: The authors declare no conflict of interest.

References

1. Wang, H.; Liu, Y.; Zhu, K. Polymetallic nodules distribution in the central pacific basin and comparison with nodules in China pioneer area, CC Zone. *Mar. Geol. Quat. Geol.* **2015**, *35*, 73–79.
2. Hein, J.R.; Spinardi, F.; Okamoto, N.; Mizell, K.; Thorburn, D.; Tawake, A. Critical metals in manganese nodules from the Cook Islands EEZ, abundances and distributions. *Ore Geol. Rev.* **2015**, *68*, 97–116. [[CrossRef](#)]
3. Battin, T.J.; Kaplan, L.A.; Findlay, S.; Hopkinson, C.; Marti, E.; Packman, A.I.; Newbold, J.D.; Sabater, F. Biophysical controls on organic carbon fluxes in fluvial networks. *Nat. Geosci.* **2008**, *1*, 95–100. [[CrossRef](#)]
4. Kristensen, E.; Kostka, J. *Macrofaunal Burrows and Irrigation in Marine Sediment: Microbiological and Biogeochemical Interactions. Interactions between Macro- and Microorganisms in Marine Sediments*; American Geophysical Union: Washington, DC, USA, 2005; pp. 125–157.
5. Villalobos, M.; Bargar, J.; Sposito, G. Sposito, Trace Metal Retention on Biogenic Manganese Oxide Nanoparticles. *Elements* **2005**, *1*, 223–226. [[CrossRef](#)]
6. De Smet, B.; Simon-Lledó, E.; Mevenkamp, L.; Pape, E.; Pasotti, F.; Jones, D.O.; Vanreusel, A. The megafauna community from an abyssal area of interest for mining of polymetallic nodules. *Deep. Sea Res. Part I Oceanogr. Res. Pap.* **2021**, *172*, 103530. [[CrossRef](#)]
7. Church, T.M.; Sarin, M.M. Chapter 2 U- and Th-Series Nuclides in the Atmosphere: Supply, Exchange, Scavenging, and Applications to Aquatic Processes. In *Radioactivity in the Environment*; Krishnaswami, S., Cochran, J.K., Eds.; Elsevier: Amsterdam, The Netherlands, 2008; pp. 11–47.
8. Steiner, Z.; Lazar, B.; Levi, S.; Tsroya, S.; Pelled, O.; Bookman, R.; Erez, J. The effect of bioturbation in pelagic sediments: Lessons from radioactive tracers and planktonic foraminifera in the Gulf of Aqaba, Red Sea. *Geochim. et Cosmochim. Acta* **2016**, *194*, 139–152. [[CrossRef](#)]
9. Yang, W.; Guo, L.; Chuang, C.-Y.; Schumann, D.; Ayrano, M.; Santschi, P.H. Adsorption characteristics of ^{210}Pb , ^{210}Po and ^7Be onto micro-particle surfaces and the effects of macromolecular organic compounds. *Geochim. et Cosmochim. Acta* **2013**, *107*, 47–64. [[CrossRef](#)]
10. Jones, D.O.B.; Kaiser, S.; Sweetman, A.K.; Smith, C.R.; Menot, L.; Vink, A.; Trueblood, D.; Greinert, J.; Billett, D.S.M.; Arbizu, P.M.; et al. Biological responses to disturbance from simulated deep-sea polymetallic nodule mining. *PLoS ONE* **2017**, *12*, e0171750. [[CrossRef](#)]
11. Cutshall, N.H.; Larsen, I.L.; Olsen, C.R. Direct analysis of ^{210}Pb in sediment samples: Self-absorption corrections. *Nucl. Instrum. Methods Phys. Res.* **1983**, *206*, 309–312. [[CrossRef](#)]
12. Dahlgard, H. Marine radioecology. In *Radioecology: Lectures in Environmental Radioactivity*; World Scientific: Singapore, 1994.

13. Smith, C.R.; Berelson, W.; Demaster, D.J.; Dobbs, F.C.; Hammond, D.; Hoover, D.J.; Pope, R.H.; Stephens, M. Latitudinal variations in benthic processes in the abyssal equatorial Pacific: Control by biogenic particle flux. *Deep. Sea Res. Part II Top. Stud. Oceanogr.* **1997**, *44*, 2295–2317. [[CrossRef](#)]
14. Smith, J.; Schafer, C. Bioturbation processes in continental slope and rise sediments delineated by Pb-210, microfossil and textural indicators. *J. Mar. Res.* **1984**, *42*, 1117–1145. [[CrossRef](#)]
15. Yan, Q.; Zhou, H. Bioturbation in near-surface sediments from the COMRA Polymetallic Nodule Area: Evidence from excess ^{210}Pb measurements. *Chin. Sci. Bull.* **2004**, *49*, 2538–2542.
16. Teal, L.R.; Bulling, M.T.; Parker, E.R.; Solan, M. Global patterns of bioturbation intensity and mixed depth of marine soft sediments. *Aquat. Biol.* **2008**, *2*, 207–218. [[CrossRef](#)]
17. Carpenter, R.; Peterson, M.; Bennett, J. ^{210}Pb -derived sediment accumulation and mixing rates for the Washington continental slope. *Mar. Geol.* **1982**, *48*, 135–164. [[CrossRef](#)]
18. Guinasso, N., Jr.; Schink, D. Quantitative estimates of biological mixing rates in abyssal sediments. *J. Geophys. Res.* **1975**, *80*, 3032–3043. [[CrossRef](#)]
19. Nozaki, Y.; Cochran, J.K.; Turekian, K.K.; Keller, G. Radiocarbon and ^{210}Pb distribution in submersible-taken deep-sea cores from Project FAMOUS. *Earth Planet. Sci. Lett.* **1977**, *34*, 167–173. [[CrossRef](#)]
20. Hyeong, K.; Seo, I.; Lee, H.-B.; Yoo, C.M.; Chi, S.-B.; Um, I.K. Variability in Particle Mixing Rates in Sediments with Polymetallic Nodules in the Equatorial Eastern Pacific as Determined from Measurements of Excess ^{210}Pb . *Ocean. Sci. J.* **2018**, *53*, 355–368. [[CrossRef](#)]
21. Lin, F.; Lin, C.; Lin, H.; Sun, X.; Lin, L. ^{210}Pb -Derived Bioturbation Rates in Sediments Around Seamounts in the Tropical Northwest Pacific. *Front. Mar. Sci.* **2021**, *8*, 701897. [[CrossRef](#)]
22. Yang, Z.; Qian, Q.; Chen, M.; Zhang, R.; Yang, W.; Zheng, M.; Qiu, Y. Enhanced but highly variable bioturbation around seamounts in the northwest Pacific. *Deep. Sea Res. Part I Oceanogr. Res. Pap.* **2019**, *156*, 103190. [[CrossRef](#)]
23. Suckow, A.; Treppke, U.; Wiedicke, M.H.; Weber, M.E. Bioturbation coefficients of deep-sea sediments from the Peru Basin determined by gamma spectrometry of $^{210}\text{Pb}_{\text{exc}}$. *Deep. Sea Res. Part II: Top. Stud. Oceanogr.* **2001**, *48*, 3569–3592. [[CrossRef](#)]
24. Froelich, P. Analysis of organic carbon in marine sediments¹. *Limnol. Oceanogr.* **1980**, *25*, 564–572.
25. Hedges, I.J.; Stern, J.H. Carbon and nitrogen determinations of carbonate-containing solids¹. *Limnol. Oceanogr.* **1984**, *29*, 657–663. [[CrossRef](#)]